NANO LETTERS

pubs.acs.org/NanoLett Letter

# Kinetically Controlled Self-Assembly of Binary Polymer-Grafted Nanocrystals into Ordered Superstructures via Solvent Vapor Annealing

Yi Wang, Jun Chen, Chenhui Zhu, Baixu Zhu, Soojin Jeong, Yi Yi, Yang Liu, Joshua Fiadorwu, Peng He, and Xingchen Ye*

Cite This: *Nano Lett.* 2021, 21, 5053−5059 Read Online

ACCESS | Metrics & More | Article Recommendations | Supporting Information

**ABSTRACT:** Polymer-inorganic nanocomposites based on polymer-grafted nanocrystals (PGNCs) are enabling technologically relevant applications owing to their unique physical, chemical, and mechanical properties. While diverse PGNC superstructures have been realized through evaporation-driven self-assembly, this approach presents multifaceted challenges in experimentally probing and controlling assembly kinetics. Here, we report a kinetically controlled assembly of binary superstructures from a homogeneous disordered PGNC mixture utilizing solvent vapor annealing (SVA). Using a $NaZn_{13}$-type superstructure as a model system, we demonstrate that varying the solvent vapor pressure during SVA allows for exquisite control of the rate and extent of PGNC assembly, providing access to nearly complete kinetic pathways of binary PGNC crystallization. Characterization of kinetically arrested intermediates reveals that assembly follows a multistep crystallization pathway involving spinodal-like preordering of PGNCs prior to $NaZn_{13}$ nucleation. Our work opens up new avenues for the synthesis of multicomponent PGNC superstructures exhibiting multifunctionalities and emergent properties through a thorough understanding of kinetic pathways.

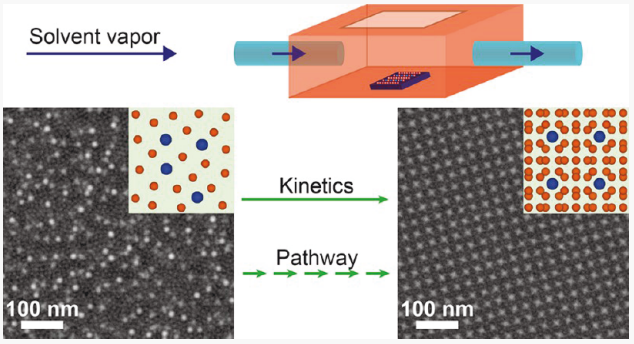


**KEYWORDS:** *polymer-grafted nanocrystals, solvent vapor annealing, kinetically controlled self-assembly, nonclassical crystallization*



Polymer-inorganic nanocomposites are enabling transformative advances in applications of photonics, plasmonics, fuel cells, photovoltaics, and nanomembranes, among others.[1−6] Assemblies of polymer-grafted nanocrystals (PGNCs) represent a modular materials platform for developing functional nanocomposites with tailored properties, versatile processability, and responsiveness to multiple stimuli.[2,7−12] Grafting polymers onto pre-synthesized nanocrystals (NCs) introduces new energetic contributions arising from the conformational entropy and interaction enthalpy of polymer chains, offering a vast parameter space for nanocomposite design.[13−19] While diverse NC and PGNC superstructures have been synthesized by evaporation-driven self-assembly,[9,20−30] it remains very challenging to study the kinetic pathways of crystallization especially for multicomponent systems. The main challenge lies in the difficulty of real-space observation of structural intermediates during disorder-to-order transitions.

Solvent vapor annealing (SVA) has been utilized extensively for controlling the morphology and ordering of polymeric materials.[31,32] Exposure to solvent vapors can swell the polymer chains and lower the glass transition temperature, thereby increasing the chain mobility. Importantly, SVA can be performed at a constant solvent vapor pressure to provide a steady thermodynamic driving force for the structure evolution and can be stopped on-demand to access the intermediate structures. Despite its proven effectiveness, there have been very few reports using SVA to synthesize NC and PGNC assemblies yet limited to one-component systems.[33−36]

Herein, we describe a kinetically controlled assembly of binary PGNCs into ordered phases using SVA. Using a $NaZn_{13}$-type superstructure as a model system, we show that varying the solvent vapor pressure during SVA provides exquisite control over the rate and extent of PGNC assembly. Furthermore, analysis of kinetically arrested intermediates reveals that the assembly follows a multistep crystallization pathway involving spinodal-like preordering of PGNCs before the nucleation and growth of $NaZn_{13}$-type crystalline domains.

**Received:** March 3, 2021
**Revised:** May 17, 2021
**Published:** June 8, 2021

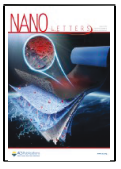

Homogeneous disordered mixtures of PGNCs were prepared by spin-coating onto Si substrates, which were solvent annealed under a range of well-defined normalized solvent vapor pressures, $p/p_0$ ($p$ and $p_0$ denote experimental and saturated solvent vapor pressures, respectively). Our custom-built SVA apparatus (Figure 1a) combines a continuous flow of

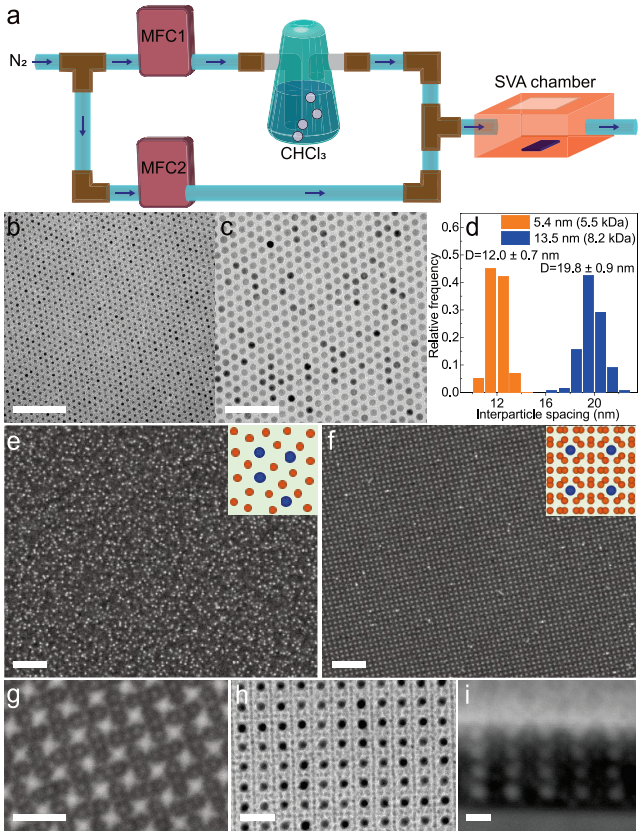


**Figure 1.** Formation of $NaZn_{13}$-type PGNC superstructure via SVA under 0.95 $p/p_0$ of $CHCl_3$ vapor. (a) Scheme of SVA setup. (b, c) TEM images of $Fe_3O_4$ PGNCs with core diameters of (b) 5.4 nm and (c) 13.5 nm. (d) Histograms of center-to-center interparticle distances of PGNCs. (e−g) Representative SEM images of binary PGNC films (e) after spin-coating and (f, g) after 15 min SVA. (h) TEM image of a binary PGNC film on the carbon-coated mica substrate after 15 min SVA. (i) Cross-sectional SEM image of $NaZn_{13}$-type superstructure. Scale bars: (b, c) 100 nm, (e, f) 200 nm, (g, h) 50 nm, (i) 20 nm.

saturated solvent vapor with a $N_2$ diluent, each regulated by a mass flow controller (MFC). Fast quenching of the solvent-swollen PGNC film (within 30 s) allowed the structures evolved after different SVA durations to be preserved and characterized. Monodisperse $Fe_3O_4$ NCs with core diameters of 5.4 and 13.5 nm were synthesized and functionalized using 5.5 kDa pentaethylenehexamine-terminated polystyrene (PS) and 8.2 kDa diethylenetriamine-terminated PS with estimated grafting densities of 0.81 and 0.56 chains/nm$^2$, respectively (Figures S1−S4 and Tables S1 and S3). Both $Fe_3O_4$ PGNCs readily formed two-dimensional hexagonal superlattices with average center-to-center interparticle distances of 12.0 and 19.8 nm (Figure 1b−d), respectively, giving rise to an effective PGNC size ratio of 0.61. One of the stable phases predicted for this size ratio is $NaZn_{13}$.[9,10,20,29,37,38]

SVA-induced disorder-to-order transition for films with a PGNC number ratio close to 13:1 was studied using scanning electron microcopy (SEM). Both top-view and cross-sectional SEM images indicate that as-spun films consisted of a disordered, random mixture of small and large PGNCs (Figure 1e and Figure S5a,b). After SVA under 0.95 $p/p_0$ $CHCl_3$ vapor for 15 min, PGNCs self-assembled into micrometer-sized ordered domains with a 4-fold symmetry (Figure 1f,g). Transmission electron microscopy (TEM) images of PGNC films prepared on carbon-coated mica substrates which were annealed under otherwise identical conditions confirm the formation of a $NaZn_{13}$-type superstructure with the [001] preferred orientation (Figure 1h). Cross-sectional SEM images reveal that the ordering persisted through the entire film thickness (Figure 1i and Figure S5g,h).

Rapid quenching of solvent-swollen films to the dry state provides an unprecedented means of studying the kinetic pathway of binary PGNC superstructure formation. Figure 2 and Figure S6 show representative SEM images of PGNC films upon SVA under 0.95 $p/p_0$ $CHCl_3$ vapor for different durations. A homogeneous disordered PGNC film first formed after spin-coating (Figure 2a). After 2 min SVA, a microscale phase-separated state was observed with distinct regions enriched with either small or large PGNCs, which resembles the morphology of typical spinodal decomposition in thin films (Figure 2b and Figure S7). The appearance of this "spinodal-like" stage is likely due to a kinetic preference for ordered small-PGNC domains rather than thermodynamically driven phase separation. The fast Fourier transform (FFT) pattern shows diffraction arcs which originate from the short-range ordered small-PGNC-rich regions. After 3 min SVA, $NaZn_{13}$-type nuclei emerged with the average dimension of ∼140 nm × 140 nm and an areal density of about 1 $\mu m^{-2}$, corresponding to an initial nucleation stage (Figure 2c). After 5 min SVA, the density of $NaZn_{13}$-type nuclei increased to ∼10 $\mu m^{-2}$ with the average domain size reaching nearly 200 nm × 200 nm, indicating a continuous nucleation stage without rapid grain growth (Figure 2d and Figure S8). The FFT pattern shows 4-fold diffraction peaks arising from the $NaZn_{13}$-type domains. From 5 to 10 min, the $NaZn_{13}$ domain size continued to increase with a concomitant reduction in domain density, corresponding to a coarsening/ripening stage where independently nucleated domains consolidated by removing grain boundaries (Figure 2e). After 15 min SVA, highly crystalline $NaZn_{13}$ superstructures formed with the majority of point defects and grain boundaries observed in the previous stage annealed out, as seen from the SEM images and the sharp and higher-order diffraction spots in the FFT pattern (Figure 2f). The formation of $NaZn_{13}$-type superstructures is robust against modest off-stoichiometries between small and large PGNCs and variations in the initial film thickness, provided that the thickness exceeds a certain threshold (Figures S9 and S10).

To complement real-space electron microscopy imaging of local structures, grazing incidence small-angle X-ray scattering (GISAXS) was employed to obtain statistically averaged information on structural order and lattice parameters. The GISAXS pattern of the as-spun film displays no Bragg diffraction peak (Figure 2g), in agreement with the disordered structure. By contrast, multiple diffraction peaks were observed in the GISAXS pattern of the PGNC film after 15 min SVA, which can be indexed to the [001]-oriented $NaZn_{13}$ phase (Figure 2h). The retrieved out-of-plane lattice constant is 45.0 nm, which is 79% of the in-plane lattice constant (57.1 nm),


https://doi.org/10.1021/acs.nanolett.1c00890
Nano Lett. 2021, 21, 5053−5059

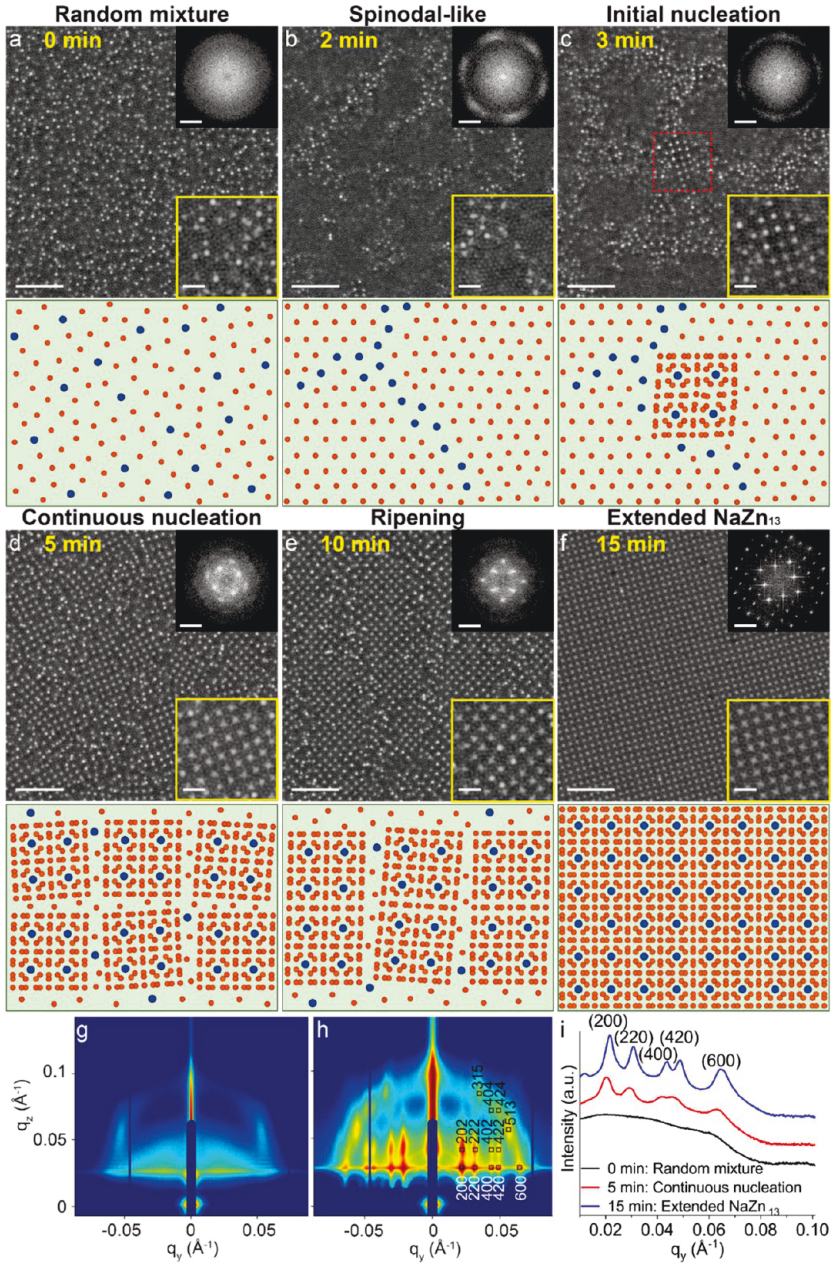


**Figure 2.** Structure evolution of a disordered mixture of PGNCs to $NaZn_{13}$-type superstructures under 0.95 $p/p_0$ of $CHCl_3$ vapor. (a–f) Low-magnification SEM images and schematic structures (main images and below), high-magnification SEM images (bottom insets), corresponding FFT patterns (top insets) of PGNC films (a) before and (b–f) after SVA for (b) 2 min, (c) 3 min, (d) 5 min, (e) 10 min, and (f) 15 min. Scale bars: (main SEM images) 200 nm, (inset SEM images) 50 nm, (FFT patterns) 0.05 $nm^{-1}$. (g, h) GISAXS patterns of PGNC films (g) before and (h) after 15 min SVA. (i) Horizontal line profiles of the GISAXS patterns along $q_z$ = 0.031 $Å^{-1}$ of the as-spun PGNC film and films after SVA for 5 and 15 min.

suggesting a lattice contraction normal to the Si substrate. We attribute this vertical contraction to the rapid deswelling of the PGNC film. Similar phenomena have been observed in other soft matter assemblies including block copolymer films and alkyl-ligand-coated NC films.[21,22,39,40] Furthermore, horizontal linecuts near the Yoneda peak reveal that the development of $NaZn_{13}$-type crystalline order preceded the superstructure densification to attain the final lattice constants (Figure 2i).

To develop a quantitative understanding of the effects of solvent vapor pressures on the assembly behavior of binary PGNCs, we monitored film thickness *in situ* using a spectroscopic reflectometer. A typical film swelling curve consists of a fast build-up step, followed by steady-state swelling and rapid deswelling to the dry state within 30 s (Figure 3a). When the relative flow rate of the saturated solvent vapor and $N_2$ diluent varied from 93/7, 85/15, 78/22 to 68/32, the solvent vapor pressure inside the SVA chamber changed from 0.95, 0.88, 0.83 to 0.74 $p/p_0$ (detailed calculations are provided in the Supporting Information). To validate our SVA setup, the thickness of pure PS films under different $p/p_0$ was measured to obtain the polymer volume fraction, $\varphi_p$, and the data were fitted using the Flory–Huggins equation[41]


https://doi.org/10.1021/acs.nanolett.1c00890
Nano Lett. 2021, 21, 5053–5059

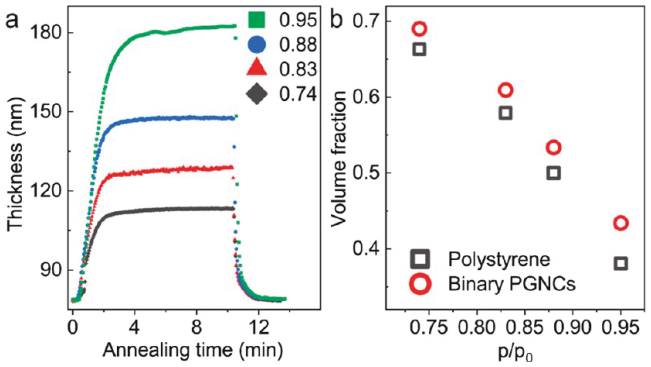


**Figure 3.** (a) Thickness profiles of binary PGNC films during SVA under different $p/p_0$ of $CHCl_3$ vapor. (b) Volume fraction of 190 kDa PS and binary PGNCs as a function of $p/p_0$ of $CHCl_3$ vapor.

$$\ln\left(\frac{p}{p_0}\right) = \chi_{P,S}\varphi_P^2 + \ln(1-\varphi_P) + \left(1-\frac{1}{N}\right)\varphi_P \quad (1)$$

where $N$ is the degree of polymerization and $\chi_{P,S}$ is the Flory–Huggins interaction parameter. The retrieved $\chi_{P,S}$ for PS/$CHCl_3$ is 0.3, in agreement with the previous literature report.[41] The volume fraction of PGNCs ($\varphi_{PGNC}$) in swollen films can be estimated as $\varphi_{PGNC} = d_0/d_{sw}$ ($d_0$ and $d_{sw}$ are dry and swollen film thickness, respectively). When $p/p_0$ was reduced from 0.95 to 0.88, 0.83, and 0.74, $\varphi_{PGNC}$ increased from 0.44 to 0.54, 0.61, and 0.69 (Figure 3b). We attribute the higher value of $\varphi_{PGNC}$ than $\varphi_P$ under identical $p/p_0$ to the nonswollen PGNC cores and different conformations between polymer brushes on PGNCs and free polymers.

The solvent vapor pressure and $\varphi_{PGNC}$ were found to play dominant roles in determining the assembly kinetics. As shown in the "time-solvent vapor pressure-transformation" diagram (Figure 4a), no superstructure formed after prolonged SVA for 300 min at 0.74 $p/p_0$ (Figure S11). The PGNC film simply swelled (up to 145% of its original thickness) and deswelled without particle reorganization. This suggests that, at such a high volume fraction ($\varphi_{PGNC}$ = 0.69), even though $NaZn_{13}$ phase is presumably still preferred, its nucleation is severely hampered because of the retarded PGNC diffusion. In the intermediate vapor pressure regime (e.g., 0.83 $p/p_0$), spinodal-like preordering of small PGNCs was observed after SVA for 15 min (Figure S12), whereas only sparsely distributed small $NaZn_{13}$-type domains (~140 nm × 140 nm, ~0.3 $\mu m^{-2}$) resulted after 90 min SVA. Therefore, the nucleation barrier of $NaZn_{13}$ phase is still high under such conditions and the grain growth is essentially suppressed. At 0.88 $p/p_0$, extended $NaZn_{13}$-type domains were obtained after 40 min SVA (Figure S13), although assembly kinetics was slower than that at 0.95 $p/p_0$. On the basis of the Phillies' model,[42] the diffusion coefficient of PGNCs decreases by nearly 50% when the solvent vapor pressure is lowered from 0.95 to 0.88 $p/p_0$ (Figure S14). Collectively, the nucleation and growth of $NaZn_{13}$-type PGNC superstructures only become kinetically facile when $\varphi_{PGNC}$ lies within the range of 0.44–0.54. The fact that lower $\varphi_{PGNC}$ resulted in faster assembly kinetics in the high-vapor-pressure regime suggests that the crystallization is

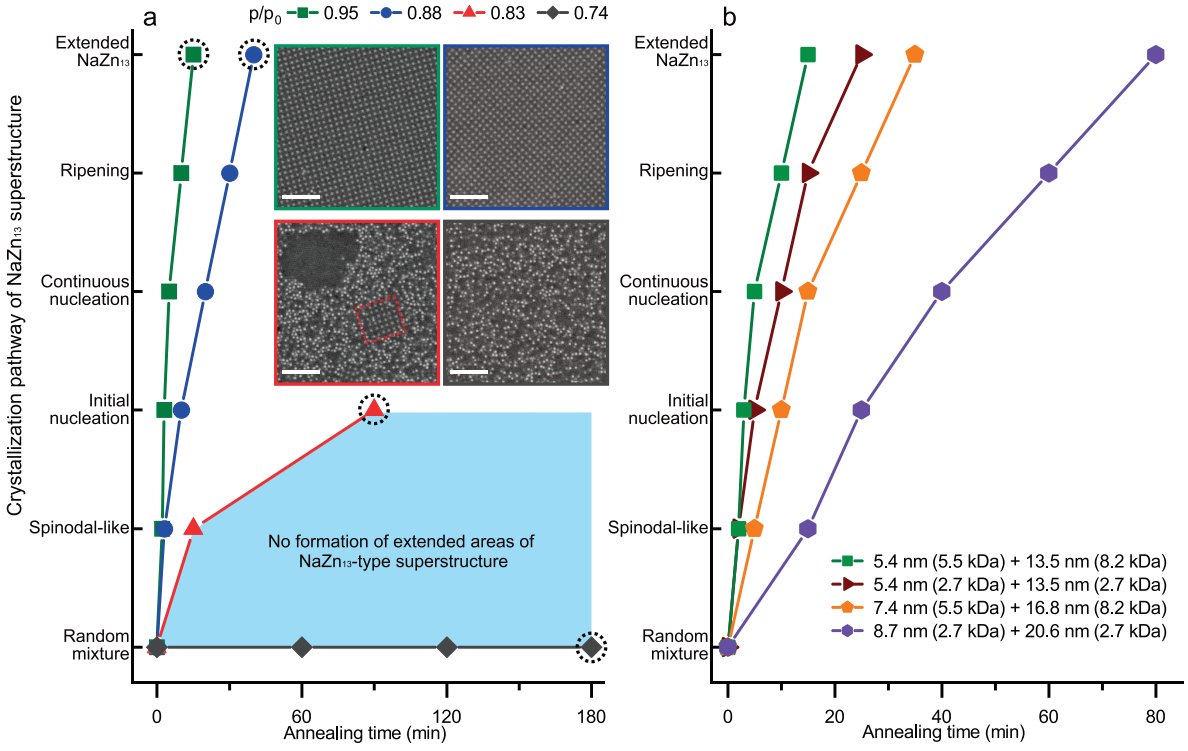


**Figure 4.** (a) Time-solvent vapor pressure-transformation diagram of binary PGNCs of 5.4 nm PS-$Fe_3O_4$ (5.5 kDa) and 13.5 nm PS-$Fe_3O_4$ (8.2 kDa) undergoing $CHCl_3$ SVA. SEM images show typical film morphologies at late stages (as indicated by the dotted circles) after SVA under different $p/p_0$ of $CHCl_3$ vapor. Scale bars: 200 nm. (b) Structure transformation diagram of binary PGNCs with different combinations of NC core sizes and grafted polymer lengths undergoing $CHCl_3$ SVA at $\varphi_{PGNC}$ = 0.44. Both graphs show the SVA times needed to reach different stages of $NaZn_{13}$ crystallization under varying experimental conditions.



https://doi.org/10.1021/acs.nanolett.1c00890
Nano Lett. 2021, 21, 5053–5059

limited by the diffusion dynamics of PGNCs rather than thermodynamic preference.

The softness of PGNCs plays an important role in dictating the kinetic pathway of superstructure formation. Of note, the range of $\varphi_{PGNC}$ (~0.44−0.54) amenable to $NaZn_{13}$ crystallization is lower than those in the theoretical predictions or previous studies on hard-sphere colloids.[43,44] For instance, a recent report on event-driven molecular dynamic simulations demonstrated that $NaZn_{13}$-type binary hard-sphere crystals can grow directly from the fluid phase at particle volume fractions of $\varphi \sim 0.565-0.590$.[43] In a pioneering study on $NaZn_{13}$ formation in suspensions of nearly hard-sphere particles, a range of $\varphi \sim 0.512-0.553$ was experimentally determined.[44] Our results indicate that distinct from colloidal hard-sphere systems, crystallization of binary PGNCs into superstructures can be feasible over a broader range of particle volume fraction with a substantially lower onset. At a constant $\varphi_{PGNC}$ of 0.44, the assembly kinetics slows down at increasing NC core sizes or decreasing grafted polymer lengths, yet still follows the same assembly pathway (Figure 4b and Figures S15−S17). Such softness-enhanced crystallization of binary phases was recently demonstrated using computer simulations.[45,46] Furthermore, our observation of spinodal-like preordering of PGNCs prior to $NaZn_{13}$ nucleation cannot be accounted for by the classical nucleation theory where nuclei having the same density and symmetry as the stable solid directly emerge from the liquid phase.[47] Instead, a multistep crystallization pathway was clearly at play, which has been increasingly recognized in various colloidal systems both experimentally and through simulations.[47−49]

In conclusion, we show that, using SVA, the structure evolution of homogeneous disordered mixtures of PGNCs to ordered superstructures can be halted on-demand and analyzed in detail. We establish that controlling the solvent vapor pressure during SVA allows for exquisite control over the rate and extent of PGNC assembly. Analysis of kinetically arrested intermediates uncovers that the crystallization of $NaZn_{13}$-type superstructures follows a multistep crystallization pathway involving spinodal-like preordering of small PGNCs prior to $NaZn_{13}$ nucleation, and the development of $NaZn_{13}$-type order precedes superstructure densification. We envision that the SVA approach is applicable to fabricating other complex PGNC superstructures including quasicrystalline assemblies.[50] Our work not only provides an effective means of forming multicomponent PGNC superstructures but also paves the way toward better understanding and ultimately controlling the kinetic pathways and superstructure selections for PGNC assemblies.

## ■ ASSOCIATED CONTENT

### Supporting Information

The Supporting Information is available free of charge at https://pubs.acs.org/doi/10.1021/acs.nanolett.1c00890.

Experimental details; materials characterization of polymers and PGNCs; additional SEM and TEM images of PGNC films after SVA under different $p/p_0$ (PDF)

## ■ AUTHOR INFORMATION


### Corresponding Author

**Xingchen Ye** − *Department of Chemistry, Indiana University, Bloomington, Indiana 47405, United States;* orcid.org/0000-0001-6851-2721; Email: xingye@indiana.edu.

### Authors

**Yi Wang** − *Department of Chemistry, Indiana University, Bloomington, Indiana 47405, United States*

**Jun Chen** − *Department of Chemistry, Indiana University, Bloomington, Indiana 47405, United States;* orcid.org/0000-0001-9173-3450

**Chenhui Zhu** − *Advanced Light Source, Lawrence Berkeley National Laboratory, Berkeley, California 94720, United States*

**Baixu Zhu** − *Department of Chemistry, Indiana University, Bloomington, Indiana 47405, United States*

**Soojin Jeong** − *Department of Chemistry, Indiana University, Bloomington, Indiana 47405, United States*

**Yi Yi** − *Department of Chemistry, Indiana University, Bloomington, Indiana 47405, United States;* orcid.org/0000-0003-3677-5126

**Yang Liu** − *Department of Chemistry, Indiana University, Bloomington, Indiana 47405, United States;* orcid.org/0000-0001-5586-623X

**Joshua Fiadorwu** − *Department of Chemistry, North Carolina Agricultural and Technical State University, Greensboro, North Carolina 27411, United States*

**Peng He** − *Department of Chemistry, North Carolina Agricultural and Technical State University, Greensboro, North Carolina 27411, United States;* orcid.org/0000-0002-4773-7566

Complete contact information is available at: https://pubs.acs.org/10.1021/acs.nanolett.1c00890



### Funding

This work was supported by the U.S. National Science Foundation (NSF DMR-2102526). P.H. and J.F acknowledge support from the Indiana University-Minority Serving Institutions STEM Summer Scholars Institute program and College of Science and Technology at North Carolina Agricultural and Technical State University. This research also made use of resources at the Advanced Light Source of Lawrence Berkeley National Laboratory, which is a DOE Office of Science User Facility supported under contract no. DE-AC02-05CH11231.


### Notes

The authors declare no competing financial interest.

## ■ ACKNOWLEDGMENTS


We thank the Indiana University Nanoscale Characterization Facility and Electron Microscopy Center for access of instrumentation.


## ■ REFERENCES


(1) Kumar, S. K.; Benicewicz, B. C.; Vaia, R. A.; Winey, K. I. 50th Anniversary Perspective: Are Polymer Nanocomposites Practical for Applications? *Macromolecules* **2017**, *50*, 714−731.

(2) Fernandes, N. J.; Koerner, H.; Giannelis, E. P.; Vaia, R. A. Hairy Nanoparticle Assemblies as One-Component Functional Polymer Nanocomposites: Opportunities and Challenges. *MRS Commun.* **2013**, *3*, 13−29.

(3) Gao, B.; Arya, G.; Tao, A. R. Self-Orienting Nanocubes for the Assembly of Plasmonic Nanojunctions. *Nat. Nanotechnol.* **2012**, *7*, 433−437.
(4) Kao, J.; Thorkelsson, K.; Bai, P.; Zhang, Z.; Sun, C.; Xu, T. Rapid Fabrication of Hierarchically Structured Supramolecular Nanocomposite Thin Films in One Minute. *Nat. Commun.* **2014**, *5*, 4053.
(5) Pastoriza-Santos, I.; Kinnear, C.; Pérez-Juste, J.; Mulvaney, P.; Liz-Marzán, L. M. Plasmonic Polymer Nanocomposites. *Nat. Rev. Mater.* **2018**, *3*, 375−391.
(6) Mueller, N. S.; Okamura, Y.; Vieira, B. G. M.; Juergensen, S.; Lange, H.; Barros, E. B.; Schulz, F.; Reich, S. Deep Strong Light-Matter Coupling in Plasmonic Nanoparticle Crystals. *Nature* **2020**, *583*, 780−784.
(7) Akcora, P.; Liu, H.; Kumar, S. K.; Moll, J.; Li, Y.; Benicewicz, B. C.; Schadler, L. S.; Acehan, D.; Panagiotopoulos, A. Z.; Pryamitsyn, V.; Ganesan, V.; Ilavsky, J.; Thiyagarajan, P.; Colby, R. H.; Douglas, J. F. Anisotropic Self-Assembly of Spherical Polymer-Grafted Nanoparticles. *Nat. Mater.* **2009**, *8*, 354−359.
(8) Ng, K. C.; Udagedara, I. B.; Rukhlenko, I. D.; Chen, Y.; Tang, Y.; Premaratne, M.; Cheng, W. Free-Standing Plasmonic-Nanorod Superlattice Sheets. *ACS Nano* **2012**, *6*, 925−934.
(9) Ye, X.; Zhu, C.; Ercius, P.; Raja, S. N.; He, B.; Jones, M. R.; Hauwiller, M. R.; Liu, Y.; Xu, T.; Alivisatos, A. P. Structural Diversity in Binary Superlattices Self-Assembled from Polymer-Grafted Nanocrystals. *Nat. Commun.* **2015**, *6*, 10052.
(10) Boles, M. A.; Engel, M.; Talapin, D. V. Self-Assembly of Colloidal Nanocrystals: From Intricate Structures to Functional Materials. *Chem. Rev.* **2016**, *116*, 11220−11289.
(11) Chancellor, A. J.; Seymour, B. T.; Zhao, B. Characterizing Polymer-Grafted Nanoparticles: From Basic Defining Parameters to Behavior in Solvents and Self-Assembled Structures. *Anal. Chem.* **2019**, *91*, 6391−6402.
(12) Yi, C.; Yang, Y.; Liu, B.; He, J.; Nie, Z. Polymer-Guided Assembly of Inorganic Nanoparticles. *Chem. Soc. Rev.* **2020**, *49*, 465−508.
(13) Dukes, D.; Li, Y.; Lewis, S.; Benicewicz, B.; Schadler, L.; Kumar, S. K. Conformational Transitions of Spherical Polymer Brushes: Synthesis, Characterization, and Theory. *Macromolecules* **2010**, *43*, 1564−1570.
(14) Choi, J.; Dong, H.; Matyjaszewski, K.; Bockstaller, M. R. Flexible Particle Array Structures by Controlling Polymer Graft Architecture. *J. Am. Chem. Soc.* **2010**, *132*, 12537−12539.
(15) Ehlert, S.; Taheri, S. M.; Pirner, D.; Drechsler, M.; Schmidt, H. W.; Förster, S. Polymer Ligand Exchange To Control Stabilization and Compatibilization of Nanocrystals. *ACS Nano* **2014**, *8*, 6114−6122.
(16) Zhang, J.; Santos, P. J.; Gabrys, P. A.; Lee, S.; Liu, C.; Macfarlane, R. J. Self-Assembling Nanocomposite Tectons. *J. Am. Chem. Soc.* **2016**, *138*, 16228−16231.
(17) Lenart, W. R.; Hore, M. J. A. Structure-Property Relationships of Polymer-Grafted Nanospheres for Designing Advanced Nanocomposites. *Nano-Struct. Nano-Objects* **2018**, *16*, 428−440.
(18) Yun, H.; Lee, Y. J.; Xu, M.; Lee, D. C.; Stein, G. E.; Kim, B. J. Softness- and Size-Dependent Packing Symmetries of Polymer-Grafted Nanoparticles. *ACS Nano* **2020**, *14*, 9644−9651.
(19) Yan, J.; Bockstaller, M. R.; Matyjaszewski, K. Brush-Modified Materials: Control of Molecular Architecture, Assembly Behavior, Properties and Applications. *Prog. Polym. Sci.* **2020**, *100*, 101180.
(20) Shevchenko, E. V.; Talapin, D. V.; Kotov, N. A.; O'Brien, S.; Murray, C. B. Structural Diversity in Binary Nanoparticle Superlattices. *Nature* **2006**, *439*, 55−59.
(21) Friedrich, H.; Gommes, C. J.; Overgaag, K.; Meeldijk, J. D.; Evers, W. H.; de Nijs, B.; Boneschanscher, M. P.; de Jongh, P. E.; Verkleij, A. J.; de Jong, K. P.; van Blaaderen, A.; Vanmaekelbergh, D. Quantitative Structural Analysis of Binary Nanocrystal Superlattices by Electron Tomography. *Nano Lett.* **2009**, *9*, 2719−2724.
(22) Smith, D. K.; Goodfellow, B.; Smilgies, D. M.; Korgel, B. A. Self-Assembled Simple Hexagonal $AB_2$ Binary Nanocrystal Superlattices: SEM, GISAXS, and Defects. *J. Am. Chem. Soc.* **2009**, *131*, 3281−3290.
(23) Dong, A.; Chen, J.; Vora, P. M.; Kikkawa, J. M.; Murray, C. B. Binary Nanocrystal Superlattice Membranes Self-Assembled at the Liquid-Air Interface. *Nature* **2010**, *466*, 474−477.
(24) Singh, G.; Chan, H.; Baskin, A.; Gelman, E.; Repnin, N.; Král, P.; Klajn, R. Self-Assembly of Magnetite Nanocubes into Helical Superstructures. *Science* **2014**, *345*, 1149−1153.
(25) Wei, J.; Schaeffer, N.; Pileni, M. P. Ligand Exchange Governs the Crystal Structures in Binary Nanocrystal Superlattices. *J. Am. Chem. Soc.* **2015**, *137*, 14773−14784.
(26) Weidman, M. C.; Smilgies, D. M.; Tisdale, W. A. Kinetics of the Self-Assembly of Nanocrystal Superlattices Measured by Real-Time in Situ X-ray Scattering. *Nat. Mater.* **2016**, *15*, 775−781.
(27) Wang, Z.; Bian, K.; Nagaoka, Y.; Fan, H.; Cao, Y. C. Regulating Multiple Variables To Understand the Nucleation and Growth and Transformation of PbS Nanocrystal Superlattices. *J. Am. Chem. Soc.* **2017**, *139*, 14476−14482.
(28) Nagaoka, Y.; Tan, R.; Li, R.; Zhu, H.; Eggert, D.; Wu, Y. A.; Liu, Y.; Wang, Z.; Chen, O. Superstructures Generated from Truncated Tetrahedral Quantum Dots. *Nature* **2018**, *561*, 378−382.
(29) Coropceanu, I.; Boles, M. A.; Talapin, D. V. Systematic Mapping of Binary Nanocrystal Superlattices: The Role of Topology in Phase Selection. *J. Am. Chem. Soc.* **2019**, *141*, 5728−5740.
(30) Udayabhaskararao, T.; Altantzis, T.; Houben, L.; Coronado-Puchau, M.; Langer, J.; Popovitz-Biro, R.; Liz-Marzan, L. M.; Vukovic, L.; Kral, P.; Bals, S.; Klajn, R. Tunable Porous Nanoallotropes Prepared by Post-Assembly Etching of Binary Nanoparticle Superlattices. *Science* **2017**, *358*, 514−518.
(31) Sinturel, C.; Vayer, M.; Morris, M.; Hillmyer, M. A. Solvent Vapor Annealing of Block Polymer Thin Films. *Macromolecules* **2013**, *46*, 5399−5415.
(32) Jin, C.; Olsen, B. C.; Luber, E. J.; Buriak, J. M. Nanopatterning via Solvent Vapor Annealing of Block Copolymer Thin Films. *Chem. Mater.* **2017**, *29*, 176−188.
(33) Bian, K.; Choi, J. J.; Kaushik, A.; Clancy, P.; Smilgies, D. M.; Hanrath, T. Shape-Anisotropy Driven Symmetry Transformations in Nanocrystal Superlattice Polymorphs. *ACS Nano* **2011**, *5*, 2815−2823.
(34) Zhang, J.; Luo, Z.; Martens, B.; Quan, Z.; Kumbhar, A.; Porter, N.; Wang, Y.; Smilgies, D. M.; Fang, J. Reversible Kirkwood-Alder Transition Observed in $Pt_3Cu_2$ Nanoctahedron Assemblies under Controlled Solvent Annealing/Drying Conditions. *J. Am. Chem. Soc.* **2012**, *134*, 14043−14049.
(35) Rupich, S. M.; Castro, F. C.; Irvine, W. T.; Talapin, D. V. Soft Epitaxy of Nanocrystal Superlattices. *Nat. Commun.* **2014**, *5*, 5045.
(36) Chen, J.; Fasoli, A.; Cushen, J. D.; Wan, L.; Ruiz, R. Self-Assembly and Directed Assembly of Polymer Grafted Nanocrystals via Solvent Annealing. *Macromolecules* **2017**, *50*, 9636−9646.
(37) Ben-Simon, A.; Eshet, H.; Rabani, E. On the Phase Behavior of Binary Mixtures of Nanoparticles. *ACS Nano* **2013**, *7*, 978−986.
(38) Travesset, A. Soft Skyrmions, Spontaneous Valence and Selection Rules in Nanoparticle Superlattices. *ACS Nano* **2017**, *11*, 5375−5382.
(39) Bosworth, J. K.; Paik, M. Y.; Ruiz, R.; Schwartz, E. L.; Huang, J. Q.; Ko, A. W.; Smilgies, D. M.; Black, C. T.; Ober, C. K. Control of Self-Assembly of Lithographically Patternable Block Copolymer Films. *ACS Nano* **2008**, *2*, 1396−1402.
(40) Hanrath, T.; Choi, J. J.; Smilgies, D. M. Structure/Processing Relationships of Highly Ordered Lead Salt Nanocrystal Superlattices. *ACS Nano* **2009**, *3*, 2975−2988.
(41) Knoll, A.; Magerle, R.; Krausch, G. Phase Behavior in Thin Films of Cylinder-Forming ABA Block Copolymers: Experiments. *J. Chem. Phys.* **2004**, *120*, 1105−1116.
(42) Phillies, G. D. J. Universal Scaling Equation for Self-Diffusion by Macromolecules in Solution. *Macromolecules* **1986**, *19*, 2367−2376.


https://doi.org/10.1021/acs.nanolett.1c00890
*Nano Lett.* 2021, 21, 5053−5059

(43) Bommineni, P. K.; Klement, M.; Engel, M. Spontaneous Crystallization in Systems of Binary Hard Sphere Colloids. *Phys. Rev. Lett.* **2020**, *124*, 218003.
(44) Bartlett, P.; Ottewill, R. H.; Pusey, P. N. Superlattice Formation in Binary Mixtures of Hard-Sphere Colloids. *Phys. Rev. Lett.* **1992**, *68*, 3801−3804.
(45) LaCour, R. A.; Adorf, C. S.; Dshemuchadse, J.; Glotzer, S. C. Influence of Softness on the Stability of Binary Colloidal Crystals. *ACS Nano* **2019**, *13*, 13829−13842.
(46) Dasgupta, T.; Coli, G. M.; Dijkstra, M. Tuning the Glass Transition: Enhanced Crystallization of the Laves Phases in Nearly Hard Spheres. *ACS Nano* **2020**, *14*, 3957−3968.
(47) Russo, J.; Tanaka, H. Nonclassical Pathways of Crystallization in Colloidal Systems. *MRS Bull.* **2016**, *41*, 369−374.
(48) De Yoreo, J. J.; Gilbert, P. U.; Sommerdijk, N. A.; Penn, R. L.; Whitelam, S.; Joester, D.; Zhang, H.; Rimer, J. D.; Navrotsky, A.; Banfield, J. F.; Wallace, A. F.; Michel, F. M.; Meldrum, F. C.; Colfen, H.; Dove, P. M. Crystallization by Particle Attachment in Synthetic, Biogenic, and Geologic Environments. *Science* **2015**, *349*, aaa6760.
(49) Ou, Z.; Wang, Z.; Luo, B.; Luijten, E.; Chen, Q. Kinetic Pathways of Crystallization at the Nanoscale. *Nat. Mater.* **2020**, *19*, 450−455.
(50) Ye, X.; Chen, J.; Irrgang, M. E.; Engel, M.; Dong, A.; Glotzer, S. C.; Murray, C. B. Quasicrystalline Nanocrystal Superlattice with Partial Matching Rules. *Nat. Mater.* **2017**, *16*, 214−219.



https://doi.org/10.1021/acs.nanolett.1c00890
*Nano Lett.* 2021, 21, 5053−5059